AIAA Meeting Papers on Disc, July 1996
A9637179, N00014-92-J-4030, AIAA Paper 96-3031

Simulations of freely propagating turbulent premixed flames

Thomas M. Smith
Georgia Inst. of Technology, Atlanta

S. Menon
Georgia Inst. of Technology, Atlanta

AIAA, ASME, SAE, and ASEE, Joint Propulsion Conference and Exhibit, 32nd, Lake Buena Vista, FL, July 1-3, 1996

The propagation rate and the structure of freely propagating premixed turbulent flames are investigated using one-dimensional simulations based on the Linear-Eddy Model (LEM) (Kerstein, 1991). Extensions to earlier models were carried out to include thermo-diffusive (Lewis number), finite-rate kinetic, and heat release effects. Reasonably good quantitative agreement in predictions of turbulent flame speed with fan-stirred bomb experiments of Abdel-Gayed et al. (1984) is obtained over most of the reported u-prime/SL range. The resulting propagation speeds are also in good agreement. Comparisons with weak-swirl burner experiments of stationary flames by Bedat and Cheng (1995) show that the model fails to predict the reported ut/SL with u-prime/SL. Reasons for the differences are discussed. (Author)

Simulations of Freely Propagating Turbulent Premixed Flames *

Thomas M. Smith† and S. Menon‡
School of Aerospace Engineering
Georgia Institute of Technology
Atlanta, GA 30332-0150

Abstract

The propagation rate and the structure of freely propagating premixed turbulent flames are investigated using one-dimensional simulations based on the Linear-Eddy Model (LEM) (Kerstein, 1991). Extensions to earlier models were carried out to include thermo-diffusive (Lewis number), finite-rate kinetic, and heat release effects. Reasonably good quantitative agreement in predictions of turbulent flame speed with fan-stirred bomb experiments of Abdel-Gayed *et al.* (1984) is obtained over most of the reported u'/S_L range. The LEM predicts the initial rapid increase in u_t/S_L with u'/S_L for low u' followed by a decreasing slope in u_t/S_L with increasing u'. Here, u_t and S_L are respectively, the turbulent and laminar flame speed and u' is the turbulence intensity. Comparisons with an earlier model based on the *"G-Equation"* (Menon and Kerstein, 1992) are also made. The resulting propagation speeds are also in good agreement. Comparisons with weak-swirl burner experiments of stationary flames by Bedat and Cheng (1995) show that the model fails to predict the reported u_t/S_L with u'/S_L. Reasons for the differences are discussed. However, progress variable probability density functions at different locations in the flame reveal the onset of distributed combustion which is predicted by the location of the flame on the Borghi combustion phase diagram (Bedat and Cheng, 1995). Finally, constant Re simulations for a range in S_L/u' compare well with experiments by Abdel-Gayed *et al.*, (1979) for low u' but predict a plateau in u_t/S_L as u' increases.

†Graduate Research Assistant, Student Member, AIAA
‡Associate Professor, Senior Member, AIAA

1 Introduction

Freely propagating premixed flames through stationary isotropic turbulence, in the absence of boundaries and external body forces though somewhat idealized, represents a fundamental flame-turbulence interaction problem encountered in many practical combustion devices such as internal combustion engines, ramjets after-burners, and industrial furnaces. Accurate prediction of characteristics such as turbulent flame speed, turbulent flame thickness, mass consumption rates, pollutant formation, turbulent flammability limits, extinction and ignition criteria are all necessary for improving the design of future combustion devices.

Prediction and analysis of propagation characteristics in complex engineering flows remains a formidable challenge. The stationary isotropic approximation simplifies the analysis of turbulence by allowing the use of well established kinetic energy inertial range scaling laws. The absence of boundaries or body forces, further simplifies the analysis and reduces the problem to a statistically one-dimensional propagation problem. The physical situation can be described as a reaction front propagating through a turbulent field separating cold reactants from hot products. The structure of the *"flame brush"* changes with turbulence r.m.s. intensity (u') and turbulent Damkohler number $D_a = \tau/\tau_c$. Here, $\tau = l/u'$ is the large-eddy turnover time, l is the integral length scale, τ_c, is the chemical time scale ($\tau_c = \delta_l/S_L$) and δ_l is the laminar flame thickness ($\delta_l = \nu/S_L$). At low u' and high D_a the front may be considered a singularly connected wrinkled *"flamelet"* with thickness equal to the laminar flame thickness. The flamelet structure is invariant to the turbulent field and thus can be considered a thin sheet with local propagation speed equal to the laminar flame speed (Peters, 1986; and Borghi, 1985). At higher u', the flame brush may

be highly convoluted and the laminar flame structure is now augmented by turbulence through the local hydrodynamic strain rate and flame surface curvature in such a way that some holes in the surface (local extinction) may appear and later disappear. The influence of strain rate and curvature are typically studied in terms of flame stretch, $(\frac{1}{\delta A}\frac{\partial \delta A}{\partial t})$ where δA is an infinitesimal flame surface area, and a Karlovitz number, K_a (a non-dimensional stretch parameter). At still higher u', the flame brush may be considered a volume of disconnected flamelets having regions of steep gradients of reacting scalars and temperature (as in the situations previously described) surrounded by regions of smoothly varying reactants, products and temperature. At very high u', the concept of distributed combustion (a volumetrically distributed combustion zone with less steep gradients) has been used to describe the flame brush. The size of the small scale turbulent eddies are of the order of, or smaller than, the flame thickness and thus, are able to increase diffusion within the flame structure. This reaction zone is much thicker than the laminar flame thickness (Bedat and Cheng, 1995).

In turbulent flows where the integral length scale is slowly varying with the turbulent Reynolds number ($Re = u'l/\nu$, and ν is the kinematic viscosity), two naturally appearing quantities which describe the influence of propagation due to burning and turbulent diffusion are the normalized turbulence intensity u'/S_L and normalized turbulent flame speed u_t/S_L (the existence of which is still being questioned). At low u', $u_t/S_L \sim (u'/S_L)^p$ where $p > 1$, and at higher levels of turbulence intensity, $u_t/S_L \sim u'/S_L$. At still higher turbulence intensities, flame stretch reduces the local burning rate and in many cases, a plateau for u_t/S_L is reached.

This functional relationship has been and continues to be the subject of many research efforts. A review of the different models of $u_t/S_L = f(u'/S_L)$ is given by Andrews and Bradley (1975) and Gulder (1990). Experimental data for u_t/S_L has been correlated in terms of turbulent Reynolds number by Abdel-Gayed *et al.* (1985) and in terms of Re and Karlovitz number by Abdel-Gayed *et al.* (1989). Recently, new approaches to modeling the propagating flame in the different combustion regimes have been introduced. Flamelet modeling using fractal geometry has been studied (Gulder, 1990). A probability density function (pdf) method that uses a transport equation for the joint pdf of a reaction progress variable and velocity has been proposed by Pope and Anand, (1984) for modeling flamelet and distributed combustion, and a model using the joint pdf of a reaction progress variable and velocity dissipation, for combustion in the flamelet regime was proposed by Pope and Cheng, (1988). Cant *et al.* (1990) proposed a pdf model for the flame surface-to-volume ratio, and Cant and Bray (1988) developed a strained laminar flamelet model using an assumed pdf shape for the reaction progress variable. A one-dimensional model for the transport of flame surface density has been proposed by Fichot *et al.* (1993), and different closure terms appearing in flame surface density models have been studied by Duclos *et al.* (1993). Hakberg and Gosman (1984) developed an analytical method for deducing u_t/S_L based on a theorem of flame propagation by Kolmogorov, Petrovsky, and Piskunov. Mantel and Borghi (1994) have developed a model of premixed wrinkled flame propagation based on a scalar dissipation equation. All these one-dimensional (1D) models are designed to not only to predict the fundamental characteristics of flames (such as u_t) but also to lead the way toward more comprehensive combustion modeling of complex engineering flows. In complex flows, the simplifying assumptions such as isotropic flow and statistically one-dimensional propagation may only be valid locally, as in the subgrid regions of Large-Eddy Simulation (LES) computational domains.

In this paper, we present a stochastic model for simulating freely propagating flames based on the Linear-Eddy Model (LEM) of Kerstein (1991). the model was originally developed as a mixing model and has shown capable of accurately simulating small scale mixing processes. As a pre-cursor to the LEM, the *"Pair Exchange"* model was used earlier by Kerstein (1986) to simulate flamelet propagation in constant density isotropic turbulence. Laminar flamelets were approximated by considering fluid cells to be a two-valued function, either fuel or product. Laminar burning proceeded by converting fuel cells adjacent to product cells, to product cells at a rate determined by the laminar flame speed and therefore, the laminar flame structure was neglected. Turbulent convection was accomplished by exchanging pairs of cells on a linear domain. The exchange process was governed by an event frequency parameter and a length scale distribution function that when combined in a stochastic simulation, yielded the correct turbulent diffusivity based on common turbulent parameters (such as u', l and Re). It was determined that u_t/S_L was strongly dependent on the turbulent

diffusivity and only weakly dependent on the large scale of turbulence. More recently, molecular diffusion and chemical kinetics processes of the LEM model were replaced by a flame propagation model based on the *"G-equation"* flamelet model (Menon and Kerstein, 1992). Results from this study showed a linear scaling between u'/S_L and u_t/S_L at high u'/S_L consistent with experimental data. However, this approach also ignored the flame structure and is not easily extended to include Lewis number and finite-rate effects.

In this study, a simulation model is described which attempts to provide a more comprehensive treatment of the turbulence-flame interactions. The present formulation is more general in nature in that it includes molecular diffusional processes, expansion due to heat release, general finite-rate kinetics and general transport phenomena. This allows us to study the effects of these mechanisms on the propagation speed and the structure of turbulent premixed flames. Qualitative comparisons with DNS using the proposed LEM with identical chemical and turbulence parameters (Smith and Menon, 1996) have demonstrated the capabilities of LEM to capture thermo-diffusive effects in freely propagating turbulent flames in spite of the one-dimensional formulation. Specifically, the LEM correctly predicts decreasing laminar flame speeds with decreasing Lewis number and increasing turbulent propagation speeds with decreasing Lewis number. The magnitude of the change in speed was found to be similar in magnitude to the change in speed predicted by DNS of freely propagating flames.

The present approach is also compared with the more computationally efficient *"G-Equation"* LEM flamelet model (Menon and Kerstein, 1992) in order to investigate the regions of applicability of the *"G-Equation"* model. Quantitative comparisons, in terms of propagation rates and turbulent flame structure, are made with Yakhot's Renormalization Group Theory (RNG) model (1988), high Reynolds number, fan-stirred bomb experiments of Abdel-Gayed *et al.* (1984), and stationary weak-swirl burner experiments of Bedat and Cheng (1995).

2 Model Formulation

The LEM is used to fully characterize the effects of turbulent diffusion on the reaction-diffusion processes in the flame zone. To resolve all the length scales, the computational domain is restricted to one dimension which is considered to be a statistical ray through the local three-dimensional (3D) flame brush in the direction of mean propagation (Kerstein, 1986). The resolution within this one-dimensional domain is chosen to resolve all the relevant length scales ranging from the integral length scale L to the smallest Kolmogorov eddy η or the laminar flame thickness, δ_l, whichever is smaller. Within this 1D domain, the equations describing constant pressure, adiabatic laminar flame propagation are:

$$\frac{\partial Y_k}{\partial t} = \frac{1}{\rho}\frac{\partial \rho Y_k V_k}{\partial x} + \frac{\dot{\omega}_k W_k}{\rho} \qquad (1)$$

$$\frac{\partial T}{\partial t} = -\frac{1}{\bar{c}_p}\sum_{k=1}^{N} c_{p,k} Y_k V_k \frac{\partial T}{\partial x} + \frac{1}{\rho \bar{c}_p}\frac{\partial}{\partial x}\left(\bar{\kappa}\frac{\partial T}{\partial x}\right) - \frac{1}{\rho \bar{c}_p}\sum_{k=1}^{N} h_k \dot{\omega}_k W_k \qquad (2)$$

and the equation of state, $p = \rho T \sum_{k=1}^{N} Y_k R_u / W_k$. Here, T, p, R_u, and ρ are respectively, temperature, pressure, universal gas constant and mass density. The *kth* species of mass fraction, molecular weight, specific heat at constant pressure, mass reaction rate, enthalpy, and diffusion velocities are respectively, Y_k, W_k, $c_{p,k}$, $\dot{\omega}_k W_k/\rho$, h_k, V_k, and N is the number of species. The species enthalpy is given by $h_k = \Delta h^o_{f,k} + \int_{T^o}^{T} c_{p,k}(T')dT'$, where $\Delta h^o_{f,k}$ is the standard heat of formation at standard temperature, T^o. The mixture averaged specific heat at constant pressure and thermal conductivity are respectively, $\bar{c}_p$ and $\bar{\kappa}$. Molecular diffusion is approximated by Fick's Law, $V_k = -(D_k/Y_k)(\partial Y_k/\partial x)$, where D_k is the mixture averaged diffusion coefficient of species k. Mass errors created by using mixture averaged diffusion coefficients are absorbed into the diluent species.

LEM incorporates turbulent stirring (convection) and laminar propagation (diffusion-reaction) separately, thus the convection terms ($u\frac{\partial T}{\partial x}$ and $u\frac{\partial Y_k}{\partial x}$) are neglected in eqs. (1) and (2). In terms of laminar flame propagation, the absence of mean convection will result in the flame propagating into the reactants, with respect to a fixed frame of reference. Physically, turbulent stirring increases the propagation rate by wrinkling (increasing) the flame surface while laminar burning acts to smoothen (decrease) the flame surface.

The LEM relates fluid element diffusivity to a random walk of a marker particle. The total turbulent

diffusion of a marker particle due to the range of eddy sizes from l to η based on *"triplet mapping"* (Kerstein, 1991) is given by:

$$D_T \approx \nu(l/\eta)^{4/3} = \frac{2}{27}\lambda \int_\eta^L l^3 f(l) dl. \qquad (3)$$

Turbulent stirring is modeled as stochastic rearrangement events which interrupt the deterministic flame propagation (solution of eqs. 1 and 2). Each rearrangement event is interpreted as the action of a single eddy on the scalar field. Three quantities govern each event: the segment (eddy) size, the location, and the rate of events. The size is determined randomly from a pdf of eddy sizes:

$$f(l) = \frac{5}{3}\frac{l^{-8/3}}{\eta^{-5/3} - L^{-5/3}} \qquad (4)$$

in the range $\eta < l < L$ (obtained from inertial range scaling (Kerstein, 1991). The event location is randomly chosen from a uniform distribution within the 1D domain, and the event rate (or frequency) is determined using an analogy between fluid dispersion in the 1D domain and turbulent diffusivity Kerstein (1991). Detailed discussions of how these parameters are determined have been reported in cited references and, therefore, are omitted here for brevity. In earlier studies, all constants appearing in the above noted scaling relations were set to unity. However, for quantitative comparison with data, calibration of these constants is required. For example, to compare LEM predictions of scalar mixing with DNS in homogeneous isotropic turbulence, the event rate was rescaled by relating the LEM diffusivity to the large-eddy turnover time in the DNS (McMurtry *et al.*, 1993). A similar procedure is carried out in the present study.

The event rate is determined as $E = \lambda X_{LEM}$, where X_{LEM} is the length of the 1D domain and λ is the event frequency per unit length having units $[L^{-1}T^{-1}]$ which is determined from (Kerstein, 1991):

$$\lambda = \frac{54}{5}\frac{\nu Re}{C_\lambda L^3}\frac{[(L/\eta)^{5/3} - 1]}{[1 - (\eta/L)^{4/3}]}. \qquad (5)$$

The time interval between events is then given as $\Delta t_{stir} = 1/(\lambda X_{LEM})$. Here, the Kolmogorov length scale is determined from the familiar inertial range scaling law $\eta = N_\eta L Re^{-3/4}$, where Re is the turbulent Reynolds number, ν is the kinematic viscosity and N_η is an empirical constant estimated by Pope, (1987) to be ~ 13, by Ronney and Yakhot, (1992) to be 10.76, and by Bradley, (1992), to be 1.28 (The effect of the choice of N_η will be discussed later). The model constant, C_λ must also be determined for the present application (discussed later).

Once the event size and location are determined and the time of the event is reached, the rearrangement event is implemented using triplet mapping (Kerstein, 1991). This mapping first creates three copies of the selected segment and then increases the spatial gradients of the copies by compressing them by a factor of three and reversing the middle copy. Finally, the original segment is replaced by the new *"mapped"* segment. The mapping event has several attributes analogous to turbulent convection. First, it is known that the flame sheet surface normal vector aligns with the most compressive strain rate direction which is mimicked by the compressive nature of the triplet mapping. Second, mapping increases the number of crossings of a single scalar value which may be interpreted as an increase in surface area due to flame wrinkling. Finally, turbulent scaling laws built into the model cause rate of strain and rate of growth of flame surface area to be of the correct order of magnitude (Kerstein, 1991). The ensemble of mapping events captures key mechanistic features of turbulent stirring despite temporally discrete representation of a time continuous process. Furthermore, omission of flame surface displacement in the other two directions (since the present model is 1D) has been shown to cause significant errors only at very low turbulence intensities where a single flame persists instead of multiple flames (Kerstein, 1986).

Propagation of a premixed flame through an isotropic turbulent field is simulated by solving eqs. (1-5) on an equally spaced discretized line. Using backward-euler time integration, second-order-accurate finite-differencing for the derivatives, and a partial decoupling strategy for the source terms (Calhoon *et al.*, 1994), the equations are marched time accurately at the diffusion time step until a statistically steady state is reached. Volumetric expansion due to heat release is implemented by expanding each linear eddy cell on the 1D line by an amount ρ_i^n/ρ_i^{n+1}, where ρ_i^n and ρ_i^{n+1} are, respectively, the density of the *ith* cell at the *n* and *n+1* time integration level. The domain containing the expanded cells is regridded so that each cell is returned to its initial volume. This increases the total number of cells; however, to maintain the same number of cells throughout the simulation (a simplification that will be discarded in

the future), a number of cells equal to the increase in the number of cells are truncated from the burnt side of the flame. Truncation is justified because the flame brush only occupies a fraction of the total domain and propagates only into the reactant mixture. Statistics describing the rate of propagation and the structure of the flame brush are only meaningful in the active regions of combustion (*i.e.* upstream of the location where cells are truncated from the domain). Since volumetric expansion is decoupled from the diffusion-reaction equations, accuracy in calculating the laminar flame speed is ensured by requiring adequate resolution of the flame and is determined by comparing $S_C = 1/\rho_0 \int_{-\infty}^{+\infty} \dot{w}_R dx$ and $S_P = \Delta x_{Y_R=0.5}/\Delta t$, where ρ_0 is the cold reactant density, $\dot{w}_R$ is the reactant reaction rate, S_C is the flame speed based on reactant mass consumption rate and S_P is the flame speed based on propagation rate of a reference mass fraction value, $Y_R = 0.5$, where $Y_R = Y_k/Y_0$ and Y_0 is the initial mass fraction of species k.

The *G-Equation* LEM models laminar burning (described previously by eqs. 1 and 2) by the propagation equation:

$$\frac{\partial G}{\partial t} = S_L |\nabla G|. \qquad (6)$$

This eq. tracks the propagation of a single value of "G" between $G_{fuel} \leq G_0 \leq G_{prod}$, where $G_{fuel} = 1$ and $G_{prod} = 0$. G_0 is a prespecified level surface representing the flame. Therefore, flame propagation is described by one scalar instead of $N + 1$ (Menon and Kerstein, 1992). The flame speed S_L is also a prespecified constant. Since there is no mathematical description of expansion due to heat release in eq. (6), expansion is implemented in terms of a physical interpretation of its effect on the "G" field. The algorithm for thermal expansion (described above) is not appropriate here since the *G-Equation* has no flame structure and therefore, no physical mechanism to compensate for the scalar profile broadening effect due to expansion. Therefore, expansion is implemented by first prescribing a reference value G_{exp} that defines a transition from fuel to product. After each time step, each new cell value, G_i^{n+1} is compared to the old value, G_i^n. If the reference value is crossed during that time step, all the heat is released, the cell is set to G_{prod} and a number $(N_{exp} - 1)$ of new G_{prod} cells are added. Here N_{exp} is the nearest integer ratio of Tp/T_f, where T_p is the product temperature and T_f is the fuel temperature. This method artificially truncates the scalar profile, increasing the gradient and therefore, may introduce artificially high burning velocities. The burning rate is determined by two methods; $S_{CG} = \sum_{i=1}^{ISGS} S_L(G_{min} - G_i)/\Delta x_{LEM}$ and $S_{PG} = \Delta x_{G_0}/\Delta t$, where G_{min} is the $min(G_{i-1}, G_i, G_{i+1})$, Δx_{LEM} is the cell size, $ISGS$ is the number of cells in the domain, X_{LEM}. In the case of laminar propagation, S_{CG} will always equal S_L however, S_{PG} may not. These flame speeds for the propagating thin front are similar to the flame speeds S_C and S_P computed for finite-rate cases. It is necessary to calculate S_{PG} even though S_L is prespecified, to ensure that the truncation introduced in the expansion algorithm does not increase the propagation rate significantly. In the *G-Equation* flames, the reference value was chosen to be 0.01 and the increase in S_{PG} due to truncation of the profile by an amount ≤ 0.01 is only of the order of 1% which is considered acceptable.

Increasing burnt cells increases relative spacing between to adjacent flames. An additional error is introduced when Tp/T_f is not an integer value; however, it has been determined that the flame front propagation rate is relatively insensitive to the amount of expansion, so the algorithm which correctly predicts the repulsion speed of two adjacent flames appears adequate.

Yakhot's RNG model is an analytical expression for the turbulent flame speed as a function of turbulence intensity ($u_t/S_L = exp[u'^2/u_i^2]$). It was derived from the *G-Field Equation* (Kerstein *et al.*, 1988) which describes the propagation of a thin flame by the actions of convection and normal burning. The model assumes no flame structure and is applicable only in the flamelet combustion regime, however, it has been shown that the model compares well with experimental data in the low to moderately high u'/S_L range. In addition, the model predicts an increasing slope (at low u'/S_L) and then decreasing slope (at high u'/S_L) in the normalized turbulent flame speed curve. Equation 6 was also obtained from the *G-Field Equation* which makes the RNG model an appropriate choice for comparisons with *G-Equation* LEM and the finite-rate model in the flamelet regime. The RNG model does not take into account D_a or K_a i effects and therefore can not predict extinction, however, Ronney *et al.*, (1992) have extended the model to include flame broadening effects at high Re. We will only compare with the model in its original form in this paper.

3 Results and Discussion

To simulate a stationary flame, a moving observation window is defined (shown in Fig. 1a) that translates with the flame brush from its original position to maintain approximately the same relative position between flame center and observation window (even though the flame propagates freely into the reactants). The extent of the flame brush is defined as the width of the domain from the *"first"* flame to the *"last"* flame with the flame center defined as the geometric center of the flame brush. The flame front location is determined by tracking a reference mass fraction $Y_R = 0.5$, that has been normalized by the initial reactant mass fraction, Y_0. As the front propagates into the reactants, and its position relative to the upstream computational boundary becomes less than a specified amount (usually one integral length scale), the observation window is shifted an equal amount to maintain approximately the same relative position. This shift requires eliminating cells from the burnt side (outflow) and adding new cells at the reactant (inflow) boundary. It was determined earlier by Menon and Kertein (1992), and in the present study, that this shift does not affect the statistics used to analyze the results. All statistics are obtained relative to the flame center. Figure 1b shows a *"snapshot"* of the flame brush. The individual profiles of Y_R represent individual flames. Note the evidence of stirring by the jagged sections of the profiles at some locations and the action of molecular diffusion by the smoothness of other profiles. Also note that the relative distance between individual flames is random in appearance.

Two chemical mechanisms are employed in this study. The first is the four-step reduced methane-air mechanism of Peters (1991):

$$\begin{aligned} CH_4 + 2H + H_2O &\rightleftharpoons CO + 4H_2 \\ CO + H_2O &\rightleftharpoons CO_2 + H_2 \\ H + H + M &\rightleftharpoons H_2 + M \\ O_2 + 3H_2 &\rightleftharpoons 2H + 2H_2O. \end{aligned}$$

that contains eight species; CH_4, H_2, O_2, H, CO, CO_2, H_2O, and N_2 (inert). The four reversible reaction rates are functions of the elementary reaction rates deduced from a forty-equation skeletal mechanism. The thermodynamic and transport data were taken directly from the CHEMKIN-II (Kee *et al.*, 1992) database. The method of evaluating thermodynamic properties such as $c_{p,k}$, h_k and mixture averaged transport coefficients such as D_k, $\bar{c}_p$, and $\bar{\kappa}$ are outlined in CHEMKIN-II, and Dufour and Soret diffusion effects have been neglected. Computational efficiency is significantly improved by *"inlining"* the transport coefficient equations directly into the code. This has been adopted for the four-step mechanism results presented here.

Laminar flame speeds for lean to moderately rich mixtures are presented in fig. 2a, and flame thickness data based on thermal thickness (defined as $\delta_{th} = (T_p - T_f)/(dT/dx)_{max}$) and based on temperature profile (defined as δ_T) are presented in fig. 2b. The LEM predictions of laminar flame properties (the simulation is carried out without turbulent stirring) are compared with the CHEMKIN-II PREMIX code, calculations by Peters (1991) and laminar flame bomb experiments by Andrews and Bradley (1972). The LEM and CHEMKIN-II predictions of flame speed, δ_{th} (fig. 2b), and δ_T (not shown) are in excellent agreement. These results demonstrate that the decoupling of expansion due to heat release in the diffusion-reaction equations does not create any significant error in the flame speed or flame thickness calculations. The differences in flame speed between our results and Peters are mainly due to the manner in which the equilibrium concentrations are obtained. Thus this is is not related to the LEM implementation of the mechanism or to any deficiency in the solution of the diffusion-reaction equations, (1) and (2). The reduced four-step mechanism has a relatively thick recombination zone which causes δ_T predicted by the four-step mechanism to be larger than the experimental results. Both LEM and CHEMKIN-II predict this behavior. However, δ_{th} compares much more closely to the experimental data (fig. 2b). Note that it is common practice to define the laminar flame thickness in terms of the laminar flame speed and the kinematic viscosity ($\delta_l = \nu/S_L$). A flame thickness defined in this manner is typically less than the thermal thickness or the temperature profile thickness.

The second mechanism studied is a single-step global decomposition mechanism; $R \Longrightarrow P$ (reactants form products) (discussed in Williams, 1985). In this case, the chemistry is described by an overall activation energy, pre-exponential factor, and product temperature. The mass rate of destruction of the normalized reactant that ranges from $[1 \rightarrow 0]$ is; $\dot{w}_R = -\rho Y_R A exp(-T_a/T)$, where T_a is the activation temperature, $T_a = E_a/R_c$, E_a is the activation energy and R_c is the universal gas constant ($R_c = 1.987\ [cal/g - mole K]$). The specific heat at

constant pressure, c_p, the Lewis number of the deficient reactant, Le, and the Prandtl number, Pr, are all assumed to be constant. The thermal conductivity is expressed as $\bar{\kappa} = c_p\mu/Pr$ and the viscosity coefficient, μ, is determined from Sutherland's Law, $\mu = \mu_o(\frac{T}{T_o})^{3/2}(\frac{T_o+S_1}{T+S_1})$, where μ_o is a reference viscosity at temperature T_o, and S_1 is a constant. The first term on the right hand side of eq. (2) is identically zero and the source terms are determined from:

$$\frac{dY_R}{dt} = \dot{w}_R/\rho \tag{7}$$

$$\frac{dT}{dt} = -\Delta h_f \dot{w}_R/(\rho c_p). \tag{8}$$

The overall activation energy is obtained by the method suggested by Abdel-Gayed *et al.* (1984). Methane-air flame data was taken directly from fig. 19 of Abdel-Gayed *et al.* (1984) (data was from laminar flame ball experiments for lean to stoichiometric flames). The slope of the line $\ln(S_L) \approx 1/2\ln(A) - (1/T_p)(T_a/2)$ is approximately equal to one half of the activation temperature T_a, and from this we determined $T_a = 14786\,[K]$, and $E_a = 29380\,[cal/g{-}mole]$ which is consistent with values suggested by Westbrook and Dryer (1981), Coffee *et al.* (1983), and Fenn *et al.* (1953).

The product temperatures for methane-air flames, were chosen from Andrews and Bradley (1972) and the pre-exponential factor was chosen so that the laminar flame speed of the stoichiometric flame matches the experimentally determined stoichiometric flame speed. Off stoichiometric flame speeds were then determined by changing the heat release by adjusting the product temperature $h_f = c_p(T_p - T_f)$. Here, the overall activation energy and the pre-exponential factor were held constant. This is not an optimum choice, since it requires that the product temperature be adjusted to compensate for the short-comings in the global mechanism. However, the results presented here illustrate the point that the single-step mechanism can capture the laminar flame speed and thickness reasonably well. The flame speed (using the correct T_p) is under predicted for very lean mixtures (fig. 2a). Nevertheless, δ_T based on 99.8% of the profile agrees reasonably well with the experimental data while δ_{th} agrees with the four-step LEM and CHEMKIN-II predictions. The laminar flame parameters used in the present study appear in Table I.

There is only one reacting species in the single-step mechanism and the reaction rate can be tabulated in terms of Y_R, T, and Δt (the diffusion time step). This produces a two-dimensional table for ΔY_R and ΔT which are defined; $\Delta Y_R = \int_t^{t+\Delta t}(\dot{w}_R/\rho)dt - Y_R^n$ and $\Delta T = \int_t^{t+\Delta t}\Delta h_f(\dot{w}_R/\rho c_p)dt - T^n$. Values are obtained from the table using bi-linear interpolation. Using the table increases computational efficiency by nearly a factor of ten compared with solving the point problem at each point in the domain and each time step. The o.d.e. solver, DVODE (part of CHEMKIN-II), is used to generate the table at the beginning of each simulation. Typical maximum relative errors in ΔY_R and ΔT are less than 0.5%.

In order to compare predictions of the turbulent flame speed with experimental data, it is necessary to determine two calibration constants. The first constant, C_λ appears in the event frequency parameter, eq. (5). This constant is introduced in order to scale the turbulent flame speed with the model turbulent diffusivity. A similar scale factor was introduced by McMurtry *et al.*, (1993) to match DNS and LEM large-eddy turnover time scales so that comparisons of scalar dissipation rates from DNS and LEM could be made. The second constant, $N_\eta > 1$ reduces the effective Re by reducing the range of scales between the integral length scale and η. It should be noted that the turbulent diffusivity, eq. (3) is not changed by N_η because in the derivation of eqs. (4) and (5), $f(l)$ is normalized by requiring $\int_\eta^L B_l f(l)dl = 1$, where B_l is a constant. Therefore, a change in N_η reflects a change in B_l and D_T remains constant.

The effect of C_λ and N_η on the normalized event frequency parameter is shown in fig. 3a. The event frequency per unit length decreases rapidly with increasing N_η and is inversely proportional to C_λ. The effect of N_η on the length scale distribution is shown in fig. 3b. The conditions chosen for these two plots were $Re = 10,000$, L/η=1000, $\nu = 1.5e^{-5}$ and represent typical values encountered in high Re flows.

The effect of these two model constants on the predicted turbulent flame speed are shown in figs. 4a and 4b, respectively. These tests were conducted using the *G-Equation* LEM, flames G1 (Table II). In fig. 4a, nine simulations were run for values of u'/S_L= 5, 15, and 25 with C_λ = 10, 15, and 20. The normalized turbulent flame speeds are compared to Yakhot's model (1988) and it is apparent that a value of C_λ in the range of $10 < C_\lambda < 15$ would closely match the present prediction with the RNG model. The constant C_λ causes an upward shift in the magnitude of u_t and a slightly increasing slope.

In fig. 4b N_η is varied for the same three u'/S_L cases as in fig. 4a. Increasing N_η only slightly increases the slope of the u_t/S_L vs. u'/S_L curve.

The turbulent flame parameters and model constants for the simulations described in this paper are given in Table II. The turbulent flame propagation speed is determined from the time trace of the propagation of the leading flame (Kerstein, 1986). Shown in fig. 5a are time traces for various simulations each with a different u'/S_L of a lean (7% CH_4 by volume) methane-air mixture from the fan-stirred bomb experiments of Abdel-Gayed *et al.* (1984). These curves correspond to flames A2 in Table II. A short initial transition time is followed by a constant propagation speed which is determined by the slope of the curve. For $u'/S_L = 1.0$ the simulation ran for roughly 10 large-eddy turnover times and for $u'/S_L = 25.0$ it ran for 243 large-eddy turnover times.

In Fig. 5b the normalized turbulent flame speed predicted by the *G-Equation* LEM flames G1, and LEM (with finite-rate) flames A1 and A2 are compared to Yakhot's model predictions. Differences between flames A1 and A2 are the model integral length scale N_η, and the number of cells required to resolve η. LEM predictions of u_t/S_L agree well with the RNG prediction for the entire range in u'/S_L. Hollow symbols in fig. 5b represent individual realizations of the fan-stirred experiments and the dotted curve is the best fit to the data given by the authors (Abdel-Gayed *et al.* 1984). Although, the LEM predictions show differences in both magnitude and shape compared to the dotted line, they are still well within the spread of the experimental data. It was reported by the authors that the flames extinguish above $u'/S_L = 25$. This feature cannot be captured with the present approach since the LEM flame brush is supported from behind by a hot bath of products, while in the experiments, the flame propagation is unsteady and a significant amount of cold reactants surrounds the initial flame kernels. It may be possible to simulate extinction using the LEM with different initial conditions and boundary conditions. This issue is currently being explored.

Two other flames, A3 and A4 were also compared with experimental data from the same apparatus. These simulations were run with different values of S_L and N_η (see Table II) but with the same C_λ, as in flames G1, A1, and A2. The turbulent flame speed predictions are less satisfactory than the predictions for flames G1, A1, and A2 which demonstrates that the model constants may be functions of S_L, Le, and/or η/δ_l. This issue is still under investigation.

Characteristics of the flame structure are examined as a function of u'/S_L in figs. 5d-5f. In fig. 5d, the radius of curvature (normalized by the expermental integral scale, $l = 0.037$ [m]) for three of the six A2 set of simulations is presented. As expected, the curvature is nearly symmetric and all three pdf's are slightly skewed to the positive side. The mean curvature decreases with increasing u'/S_L. The probability of large radii of curvature decreases with increasing u'/S_L because as u' increases, the probability distribution of eddy sizes shifts to smaller eddies and therefore, the small scales are more frequently chosen for the stirring event. There is a slightly increased probability in the positive tail region for all three cases. This increased probability is due to laminar propagation and thermal expansion, both increase the radius of curvature. However, this slight increase is almost completely nullified by the high turbulence intensity at $u'/S_L = 25$.

In fig. 5e, the LEM flame surface density for all six simulations is presented. The flame surface density is calculated by time averaging the number of flames (defined as a scalar crossing of $Y_R = 0.5$) at a location relative to the flame center. The plot has been cropped at the top to accentuate the flame structure. The spike in all six cases (which reduces as u'/S_L increases) is present because there are times when only one flame is in the domain and it will be located at the flame center so the average number of flames will be highest there. The flame surface density ranges from 2.5 to 5.0 integral scales over the range in u'/S_L. The shape of the flame brush is nearly symmetric. Figure 5f is a plot of the reactant consumption rate. Its character is very representative of the flame brush. The width of the reaction zone increases with u'/S_L, and its shape is nearly symmetric about the flame center.

The LEM was also compared to the weak-swirl burner flame data of Bedat and Cheng (1995), (see Table I and II, flames B1-B4). The weak-swirl burner creates a slightly diverging flow on the periphery of the outer co-flowing jet. The inner jet contains a nearly isotropic turbulent flow generated by a grid followed by a convergent nozzle upstream of the burner lip. The divergent flow stays mainly on the periphery, creating on the burner axis a decelerating flow so that a stable flame front is achieved. Four flames were investigated: two in the corrugated flamelet regime and two in the distributed combustion regime. The LEM model using the $R \Longrightarrow P$ mechanism with constant

pre-exponential factor and activation energy was calibrated for Case I with T_p obtained from Andrews and Bradley (1972) data. The laminar flame speed of the other three flames were determined by varying T_p until the reported value was achieved. This results in slightly higher temperatures for the $\phi = 0.6$ and $\phi = 0.65$ cases. The authors report for u'/S_L= 1.8, 5.0, 8.8, and 11.5 that u_t/S_L=4.7, 10.3, 18.1, and 24.5, respectively. The LEM predictions for the same u'/S_L are u_t/S_L=4.587, 6.444, 6.361, and 7.307.

The experimentally obtained turbulent flame brush thicknesses range between 0.0255 and 0.035 [m]. The LEM flame brush thickness based on the progress variable range $0.1 \leq < C > \leq 0.9$ is 0.015 to 0.01665 [m] which is roughly one integral length scale and half of the values reported by the authors. However, it is not known how this quantity was measured and the authors report that the flames bounced. It is unclear how flame bouncing affects the flame speed and flame brush width measurements.

The pdf of the progress variable, $< C >$, where $C = 1 - Y_R$ and the variance of $< C^2 >^{1/2}$ are shown for two cases on fig. 6a. The pdf's of C for five different locations in the flame (determined from $< C >$) for flames B1 and B4 are plotted in figs. 6b and 6c. The pdf's are constructed by first calculating the $< C >$ profile and then defining a $\Delta_{<C>}$ width of 0.1 and then creating a histogram. The histogram is normalized to obtain the desired pdf. Figure 6b for flame B1 clearly shows that the combustion is composed mainly of flamelets by the sharply defined bi-modal peaks in the pdf. On the other hand, in fig 6c, flame B4 shows much higher probabilities of intermediate values of C, especially near the flame front.

The Borghi combustion phase diagram is a theoretical plot of u'/S_L vs. l/δ_l which is used to describe different regimes of premixed combustion. It also contains clearly defined boundaries for the different regimes (however, distinct boundaries may not exist). According the the Borghi diagram, B1 is placed in the corrugated flamelet regime and B4 is well within the distributed reaction zone regime. Therefore, it is possible that the increased probability of the progress variable not equal to zero or one, seen in fig. 6c is due to distributed reaction zones.

The value of activation energy used in the model mainly determines the laminar flame thickness. The parameter η/δ_l appearing in the turbulent D_a is needed to define the combustion regime. Six flames were simulated, B5, B1, and B6, corresponding to Case I turbulent flow parameters and B7, B4, and B8, corresponding to Case IV of Bedat and Cheng (1995). The first three flames have $S_L = 0.30$ with different pre-exponential factors and different activation energies, while the second set of three flames have $S_L = 0.15$. The lowest activation energy, $E_a = 9652\ [cal/g - mole]$ was extrapolated from Table I of Abdel-Gayed *et al.* (1984), using T_a and S_L from the 8.5% and 7% CH_4 flame data and the highest activation energy $E_a = 36421\ [cal/g - mole]$ was obtained by extrapolating in terms of % concentration using the same data. These two extrapolation methods are admittedly crude, compared to the method used earlier (see discussion on fig. 2a and 2b). Although, these activation energies are considered reasonable it will be shown that this choice effects the turbulent flame speed. The flame propagation time traces of the simulations are shown on figs. 7a and 7b. In fig. 7a, $u'/S_L = 1.8$ and the traces of all three flames are nearly the same. However, in fig. 7b, $u'/S_L = 11.33$ and flame B7 has a significantly higher flame speed than the other two flames, B4 and B8. An order of magnitude difference in D_a, 162 for the flames B5, B1, and B6 and 12 for flames B7, B4, and B8 may explain why the turbulent flame speed varies in this manner for the low S_L simulations.

In fig. 8, results from simulations of four different Re are presented. Flame B1, B4, B9, and B10 were simulated at four different u'. The normalized turbulent flame speed is plotted for constant Re against S_L/u'. The data shows agreement in the general trends seen by Abdel-Gayed *et al.* (1979), at low turbulence intensity. The curves seem to collapse as S_L/u' increases. However, as u' increases, the LEM flame u_t/S_L reaches a plateau and as u' increases further, u_t/S_L tends toward zero. This may be the result of turbulent diffusion. As S_L decreases, the flame thickness generally increases so as S_L/u' decreases, the ratio η/δ_l decreases. This would indicate that the turbulent diffusivity is becoming more important in the flame structure. The affect of small scale stirring may affect the propagation rate through the redistribution of heat by the action of turbulent diffusion, causing a reduction in the overall reaction rates within the flame.

4 Conclusions

The structure and propagation characteristics of turbulent premixed flames have been investigated using

one-dimensional simulations based on the linear-eddy model LEM (Kerstein, 1991). Extensions to an earlier LEM model were carried out to include finite-rate kinetics, thermo-diffusive, and heat release effects. LEM predictions of u_t/S_L are in good agreement with Yakhot's (1988) model over a wide range in u'/S_L. Reasonable quantitative agreement with high-Re experiments are also obtained. The rapid increase of u_t/S_L with increase in the normalized turbulence intensity at low u'/S_L followed by the bending of the curve at higher u'/S_L is reproduced. The LEM-analog of the flame surface density shows that the flame area and width of the flame brush increases with an increase in u'/S_L. The pdf of flame radius of curvature is nearly symmetric and the mean radius decreases with increasing u'/S_L. Comparisons with an earlier model based on the *"G-Equation"* (Menon and Kerstein 1992) show that the predictions of the propagation speeds are in good agreement.

The LEM fails to predict the turbulent flame speed of the weak-swirl burner experiments of Bedat and Cheng (1995), however, the flame brush width is predicted to within a factor of two and the pdf's of the progress variable at different locations within the flame show the onset of distributed combustion in agreement with the Borghi phase diagram. Simulations designed to evaluate the sensitivity of the activation energy demonstrate the model's capability predict propagation rate trends based on Damkohler number.

Trends in u_t/S_L based on S_L/u' for different Re are also captured by the model. The normalized turbulent flame speed decreases with increasing S_L/u' in agreement with experimental data by Abdel-Gayed *et al.*, (1979), but at low S_L/u' (high u') the LEM predicts a plateau in u_t/S_L.

These results demonstrate that the LEM approach can capture many underlying features of the premixed flame and is capable of predicting the turbulent flame speed. The demonstration that the LEM can be used to study high Reynolds number premixed flames may make this simulation model a valuable tool for analyzing turbulent premixed flames. Further work is needed to describe the functional form of model constants.

Acknowledgments

This work was supported in part by the Office of Naval Research grant N00014-92-J-4030. Support for the DNS computations was provided by the DOD HPC Center at Wright Patterson AFB.

References

Abdel-Gayed, R. G., Bradley, D., and McMahon, M. (1979) "Turbulent Flame Propagation in Premixed Gases: Theory and Experiment," *Seventeenth Symposium (International) on Combustion* The Combustion Institute, Pittsburgh, pp. 245-254.

Abdel-Gayed, R. G., Al-Khishali, K. J. and Bradley, D., (1984) "Turbulent Burning Velocities and Flame Straining in Explosions," *Proc. R. Soc. Lond.* A 39, pp. 393-44.

Abdel-Gayed, R. G. and Bradley, D, (1985) "Criteria for Turbulent Propagation Limits of Premixed Flames," *Combust. Flame* 62: 6-68.

Abdel-Gayed, R. G. and Bradley, D, (1989) "Combustion Regimes and the Straining of Turbulent Premixed Flames," *Combust. Flame* 76: 23-28 (1989).

Andrews, G. E., Bradley, D. and Lwakabamba, S. B., (1975) Turbulence and Turbulent Flame Propagation-A Critical Appraisal," *Combust. Flame* 24: 285-304.

Andrews, G. E., Bradley, D., (1972) "The Burning Velocity of Methane-Air Mixtures," *Combust. Flame* 6: 275-288.

Bedat, b. and Cheng, R. K. (1995) "Experimental Study of Premixed Flames in Intense Isotropic Turbulence," *Combust. Flame* 00: 486-494.

Borghi, R. (1985) "On the Structure and Morphology of Turbulent Premixed Flames," in Recent Advances in Aerospace Sciences, eds. Casci, C. and Bruno, C., Plenum Press, pp. 7-38.

Bradley, D. (1992) "How Fast Can We Burn," *Twentieth-Fourth Symposium (International) on Combustion*, The Combustion Institute, Pittsburgh, pp. 247-262.

Calhoon, W. H., Menon, S. and Goldin, G., (1995) "Comparison of Reduced and Full Chemical Mech-

anisms for Nonpremixed Turbulent H_2-Air Jet Flames," *Combust. Sci. Tech.*, Vol. 04, pp. 5-4.

Cant, R. S. and Bray, K. N. C. (1988) "Strained Laminar Flamelet Calculations of Premixed Turbulent Combustion In A Closed Vessel," *Twenty-Second Symposium (International) on Combustion*, The Combustion Institute, Pittsburgh, pp. 79-799.

Cant, R. S.. Pope, S. B., and Bray, K. N. C. (1990) "Modelling of Flamelet Surface-To-Volume Ratio In Turbulent Premixed Combustion, " *Twenty-Third Symposium (International) on Combustion*, The Combustion Institute, Pittsburgh, pp. 809-85.

Coffee, T. P., Kotlar, A. J. and Miller, M. S. (1983) "The Overall Reaction Concept in Premixed, Laminar, Steady-State Flames. I. Stoichiometries," *Combust. Flame*, 54: 55-69.

Duclos, J. M., Veynante, D. and Poinsot, T. (1993) "A Comparison of Flamelet Models for Premixed Turbulent Combustion," *Combust. Flame* 95: 0-7.

Fenn, J. B. and Calcote, H. F. (1953) "Activation Energies in High Temperature Combustion," Fourth Symposium on Combustion, Flame and Explosion Phenomena, The Williams and Wilkins Co., pp. 23-239.

Fichot, F., Lacas, F., Veynante, D. and Candel, S. (1993) "One-Dimensional Propagation of a Premixed Turbulent Flame With a Balance Equation for the Flame Surface Density," *Combust. Sci. Tech.*, Vol. 90, pp. 35-60.

Gulder, O. L. (1990) "Turbulent Premixed Combustion Modelling Using Fractal Geometry," *Twenty-Third Symposium (International) on Combustion*, The Combustion Institute, Pittsburgh, pp. 835-842.

Gulder, O. L. (1990) "Turbulent Premixed Flame Propagation Models for Different Combustion Regimes," *Twenty-Third Symposium (International) on Combustion*, The Combustion Institute, Pittsburgh, pp. 743-750.

Hakberg, B. and Gosman, A. D. (1984) "Analytical Determination of Turbulent Flame Speed from Combustion Models," *Twentieth Symposium (International) on Combustion*, The Combustion Institute, Pittsburgh, pp. 225-232.

Kee, J. R., Rupley, F. M., and Miller, J. A.,(1992) "CHEMKIN-II A Fortran Chemical Kinetics Package for the Analysis of Gas Phase Chemical Kinetics," SAND89-8009B, April.

Kerstein, A. R., (1986) "Pair-Exchange Model of Turbulent Premixed Flame Propagation," *Twenty-first Symposium (International) on Combustion*, The Combustion Institute, Pittsburgh, pp. 28-289.

Kerstein, A. R., Ashurst, Wm. T., and Williams, F. A.(1988) "The Field Equation for interface Propagation in an Unsteady Homogeneous Flow Field," *Phys. Rev.* A. 37, pp. 2728-2731.

Kerstein, A. R., (1991) "Linear-Eddy Modeling of Turbulent Transport. Part 6. Microstructure of Diffusive Scalar Mixing Fields," *J. Fluid Mech.* Vol. 23 p. 36.

Kerstein, A. R., (1992) *Combust. Sci. Tech.* Vol. 8, 75-86.

Mantel, T. and Borghi, R. (1994) "A New Model of Premixed Wrinkled Flame Propagation Based on a Scalar Dissipation Equation, " *Combust. Flame* 96: 443-457.

McMurtry, P. A. Gansauge, T. C., Kerstein, A. R., and Krueger, S. K., (1993) "Linear-Eddy Simulations of Mixing in a Homogeneous turbulent Flow," Phys. Fluids A 5: 023-034.

Menon, S. and Kerstein, A. R., (1992) "Stochastic Simulation of the Structure and Propagation Rate of Turbulent Premixed Flames," *Twenty-Fourth Symposium (International) on Combustion*, The Combustion Institute, Pittsburgh, pp. 443-450.

Peters, N. (1986) "Laminar Flamelet Concepts in Turbulent Combustion," *Twenty-First Symposium (International) on Combustion*, The Combustion Institute, Pittsburgh, pp. 23-250.

Peters, N. (1991) "Reducing Mechanisms," in Lecture Notes in Physics, Smooke, M.D. ed. Springer-Verlag, 384, pp. 48-67.

Pope, S. B. and Anand, M. S. (1984) "Flamelet and Distributed Combustion in Premixed Turbulent Flames," *Twentieth Symposium (International) on Combustion*, The Combustion Institute, Pittsburgh, pp. 403-40.

Pope, S. B., (1987) "Turbulent Premixed Flames," *Ann. Rev. Fluid Mech.*, pp. 237-270.

Pope, S. B. and Cheng, W. K. (1988) "The Stochastic Flamelet Model of Turbulent Premixed Combustion," *Twenty-Second Symposium (International) on Combustion*, The Combustion Institute, Pittsburgh, pp. 78-789.

Ronney, P. D., and Yakhot, V. (1992) "Flame Broadening Effects on Premixed Turbulent Flame Speed," *Combust. Sci. Tech.*, Vol. 86, pp. 3-43.

Smith, T. M. and Menon, S., (1996) "Model Simulations of Freely Propagating Turbulent Premixed Flames," *to be presented at the Twenty-Sixth Symposium (International) on Combustion*, The Combustion Institute, Pittsburgh.

Westbrook, C. K. and Dryer, F. L. (1981) "Simplified Reaction Mechanisms for the Oxidation of Hydrocarbon Fuels in Flames," *Combust. Sci. Tech.*, Vol. 27, pp. 3-43.

Williams, F. A., (1985) Combustion Theory, 2nd ed., Benjamin-Cummings, Menlo Park, pp. 429-436.

Yakhot, V., (1988) "Propagation Velocity of Premixed Turbulent Flames," *Combust. Sci. Tech.*, 60, pp. 9-24.

Table I. Laminar Flame Properties.

Flame	S_L $[m/sec.]$	δ_{th}x10^4 $[m]$	νx10^6 $[m^2/sec.]$	Le	A $[sec.^{-1}]$	E_a $[cal/g-mol]$	T_f [K]	T_p [K]	ϕ
A1	0.36	2.97	18.08	0.973	5.55e9	36422	328	1898	0.717
A2	0.36	2.97	18.08	0.973	5.55e9	36422	328	1898	0.717
A3	0.17	5.60	15.7	0.97	3.368e8	29380	298	1750	0.638
A4	0.30	4.14	17.61	2.03	4.55e6	17486	328	1900	0.70
B1	0.30	3.62	16.0	0.97	3.01e8	29380	300	2003	0.80
B2	0.18	5.47	16.0	0.97	3.01e8	29380	300	1789	0.65
B3	0.15	6.37	16.0	0.97	3.01e8	29380	300	1721	0.60
B4	0.15	6.37	16.0	0.97	3.01e8	29380	300	1721	0.60
B5	0.30	5.30	16.0	0.97	2.736e5	9652	300	2003	0.80
B6	0.30	3.45	16.0	0.97	2.641e9	36421	300	2003	0.80
B7	0.15	9.27	16.0	0.97	1.178e5	9652	300	1721	0.60
B8	0.15	6.10	16.0	0.97	3.532e9	36421	300	1721	0.60
B9	0.406	2.85	16.0	0.97	3.01e8	29380	300	2154	0.95
B10	0.4509	2.64	16.0	0.97	3.01e8	29380	300	2210	1.1

Table II. Turbulent Flame Properties.

Flame	Re	u' $[m/sec.]$	L $[m]$	u'/S_L	u_t $[m/sec.]$	u_t/S_L	X_{LEM} $[m]$	# cells	C_λ	N_η
A1	737-18418	0.36-10.8	0.037	1-30	0.61-6.58	1.7-18.27	0.305	12200	15	10.76
A2	3544-88606	0.36-9.0	0.178	1-25	.54-5.03	1.51-13.97	0.305	16385	15	3.25
A3	1927-28911	0.17-2.55	0.178	1-15	.24-1.29	1.39-7.58	0.305	16385	15	1.4
A4	3032-60647	0.30-6.0	0.178	1-20	.49-2.37	1.63-7.89	0.305	16385	15	2.43
B1	488-2112	0.52-2.25	0.015	1.8-7.5	1.38-3.38	4.587-11.27	0.055	2816	3.5	2
B2	835	.89	0.015	5.0	1.16	6.44	0.055	2816	3.5	2
B3	1220	1.30	0.015	8.8	0.96	6.36	0.055	2816	3.5	2
B4	488-2112	0.52-2.25	0.015	3.47-15	0.74-1.16	4.96-7.75	0.055	2816	3.5	2
B5	488	0.52	0.015	1.73	1.425	4.75	0.055	2816	3.5	2
B6	488	0.52	0.015	1.73	1.39	4.64	0.055	2816	3.5	2
B7	1594	1.7	0.015	11.3	1.32	8.78	0.055	2816	3.5	2
B8	1594	1.7	0.015	11.3	1.07	7.13	0.055	2816	3.5	2
B9	488-1594	0.52-2.25	0.015	1.28-4.19	1.62-10.21	4.0-10.21	0.055	2816	3.5	2
B10	488-2112	0.52-2.25	0.015	1.15-4.99	1.7-5.46	3.78-12.12	0.055	2816	3.5	2
G1	3544-88606	0.36-9.0	0.178	1-25	.54-5.03	1.51-13.97	0.305	16385	15	3.25

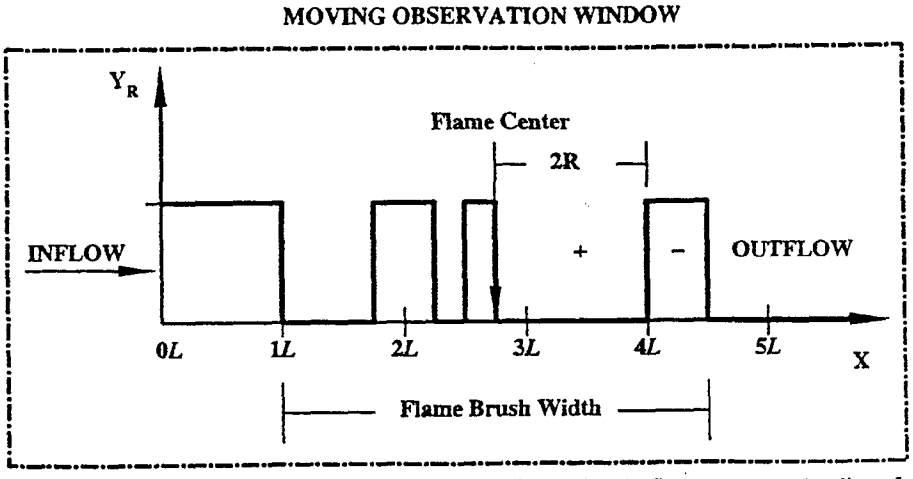

Fig. 1a. Schematic diagram of the LEM simulation domain. Flame brush, flame center and radius of curvature are also defined.

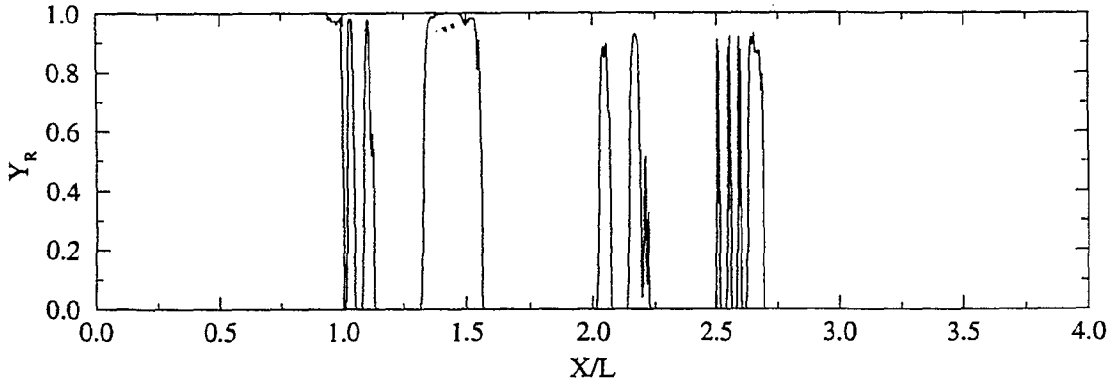

Fig. 1b. Snapshot of the flame brush in terms of normalized mass fraction for u'/S_L=30.

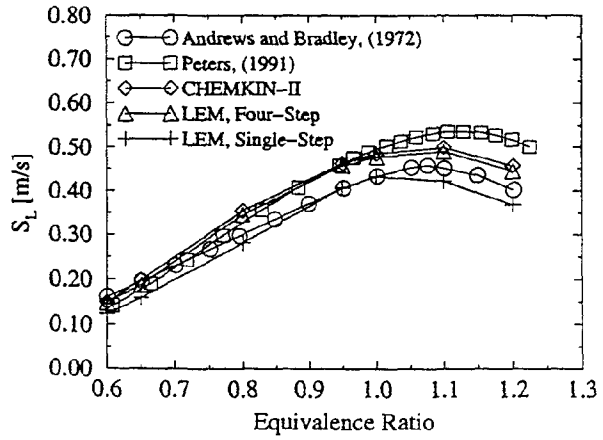

Fig. 2a. Laminar flame speed as a function of equivalence ratio for methane–air mixtures.

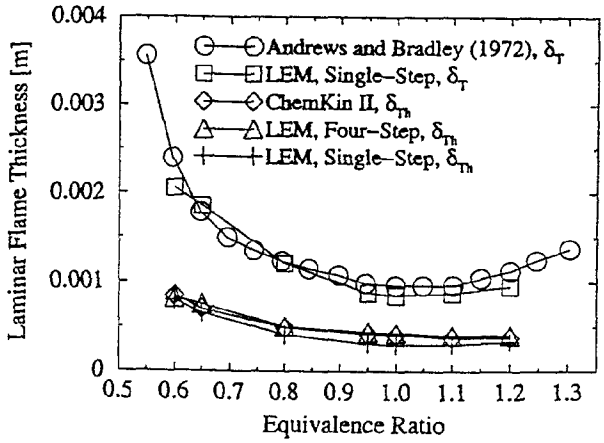

Fig. 2b. Laminar flame thickness as a function of equivalence ratio for methane–air mixtures.

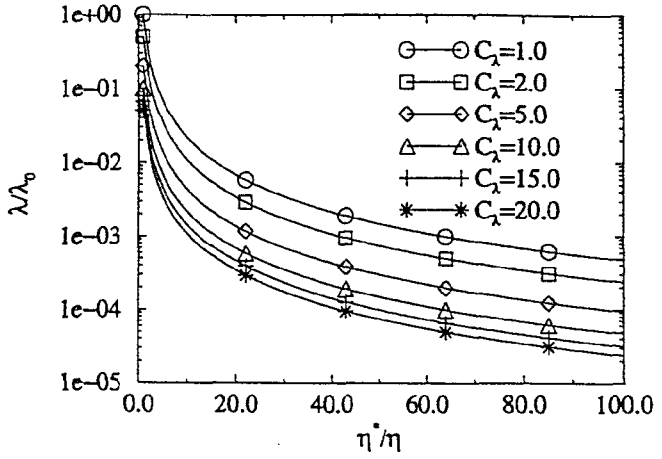

Fig. 3a. Normalized stirring rate parameter for different stirring rate constants, C_λ, as a function of N_η.

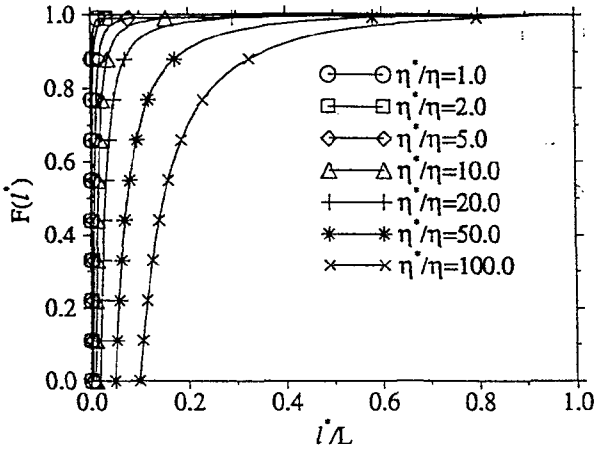

Fig. 3b. Distribution function of eddy sizes chosen for stirring events.

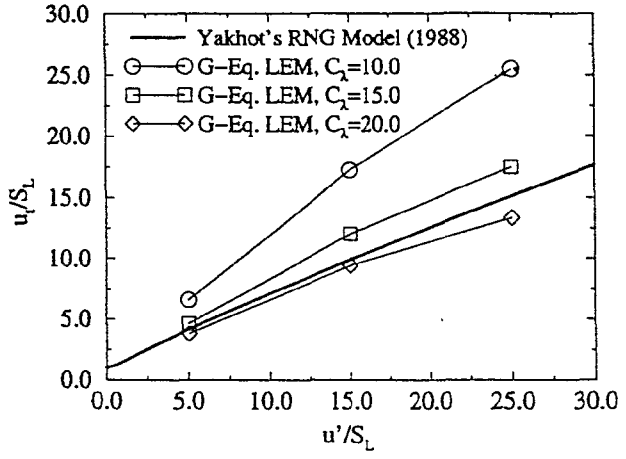

Fig. 4a. Normalized turbulent flame speed as a function of normalized turbulence intensity, predicted by G–LEM, for different stirring rate constants, C_λ.

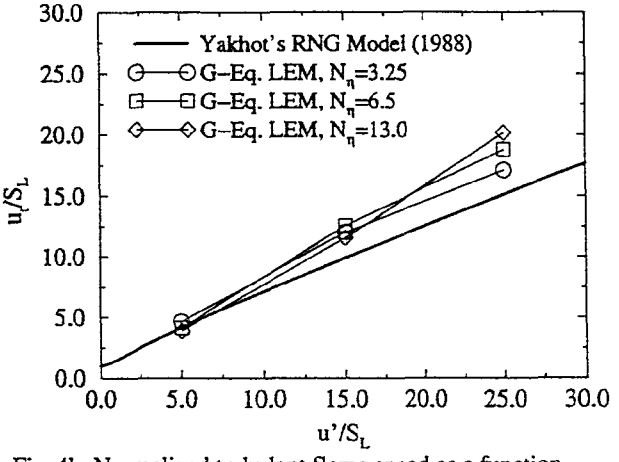

Fig. 4b. Normalized turbulent flame speed as a function of normalized turbulence intensity, predicted by G–LEM for different model constants, N_η.

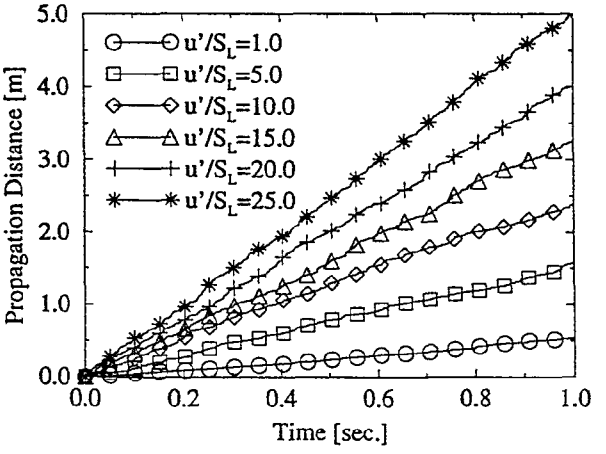

Fig. 5a. Time trace of flame front propagation of flames A2 for different u'/S_L.

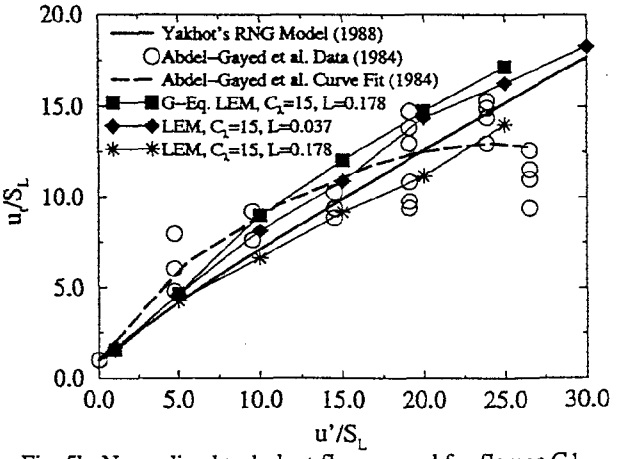

Fig. 5b. Normalized turbulent flame speed for flames G1, A1, and A2, compared with Yakhot's model, (1988), and fan–stirred bomb experiments of Abdel–Gayed *et al.*, (1984).

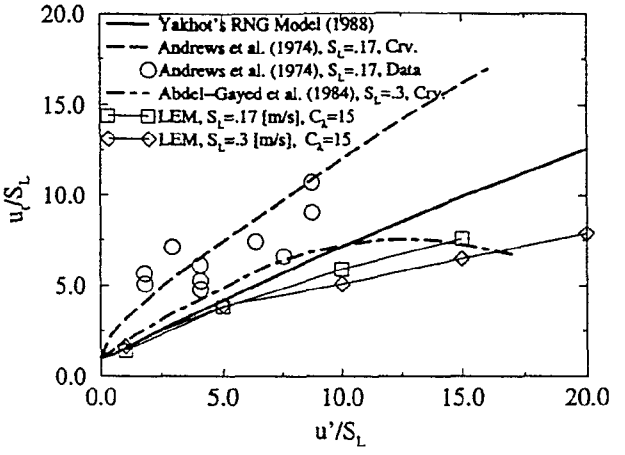

Fig. 5c. Normalized turbulent flame speed, for flames A3 and A4, compared with Yakhot's (1988), model and fan-stirred bomb experimnents of Andrews *et al.*, (1974), and Abdel-Gayed *et al.*, (1984).

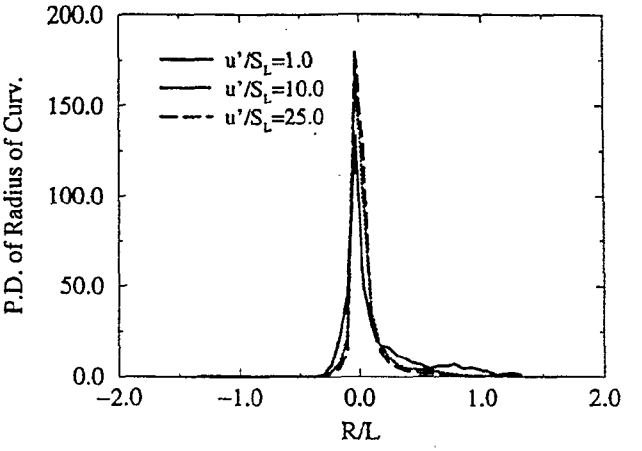

Fig. 5d. Probability density of radius of curvature of flames A2, for different u'/S_L.

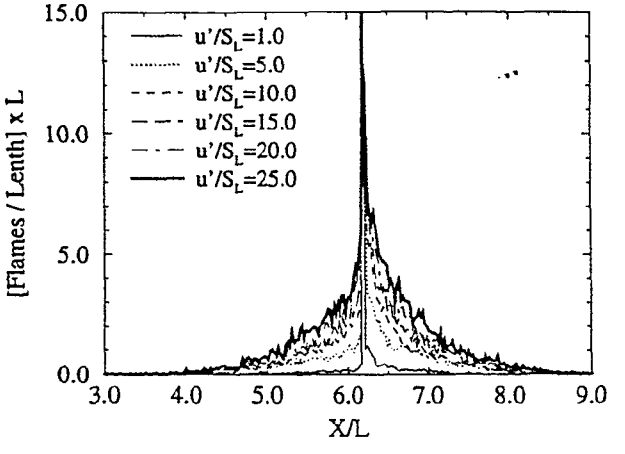

Fig. 5e. LEM flame surface density of flames A2, for different u'/S_L.

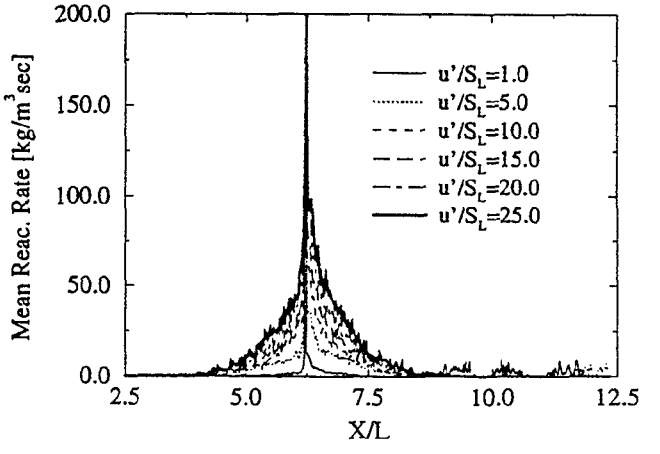

Fig. 5f. Mean mass reactant consumption rate of flames A2, for different u'/S_L.

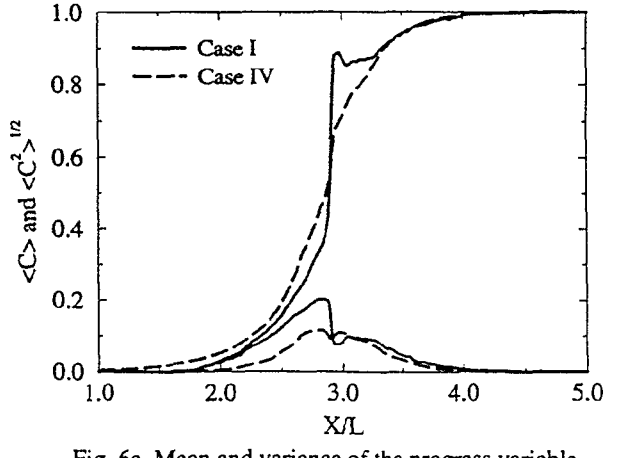

Fig. 6a. Mean and variance of the progress variable ($C=1-Y_R$) for flames B1 and B4.

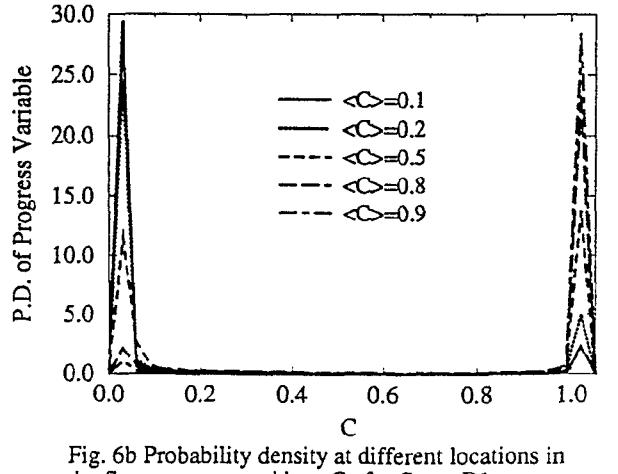

Fig. 6b Probability density at different locations in the flame represented by <C> for flame B1, corresponding to Case I of Bedat and Cheng (1995).

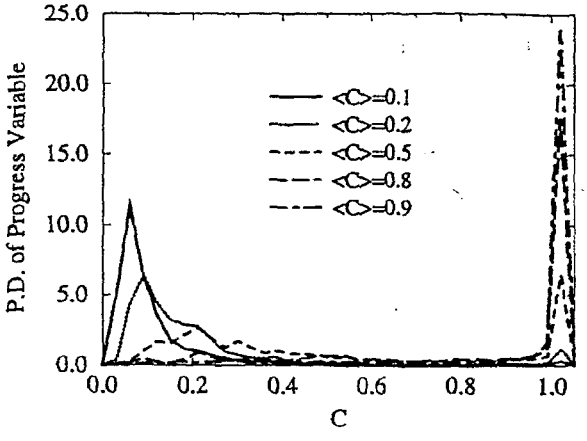

Fig. 6c Probability density at different locations in the flame represented by <C> for flame B4, corresponding to Case 4 of Bedat and Cheng (1995).

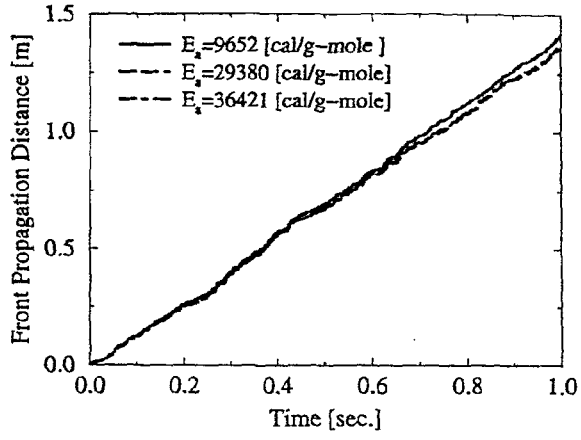

Fig. 7a. Time trace of flame front propagation for flames B5, B1, and B6 with u'/S_L=1.8 and S_L=0.30, for different activation energies.

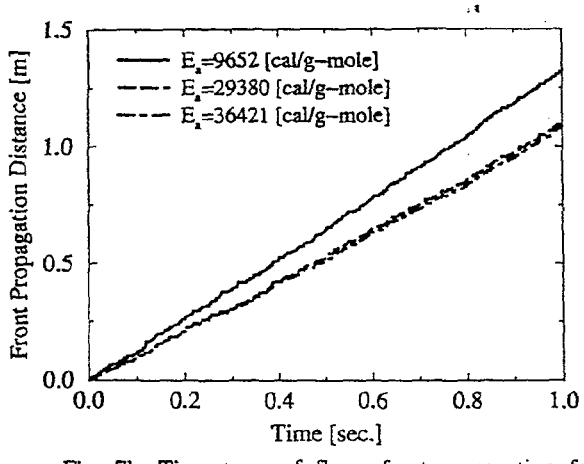

Fig. 7b. Time trace of flame front propagation for flames B7, B4, and B8 with u'/S_L=11.3 and S_L=0.15, for different activation energies.

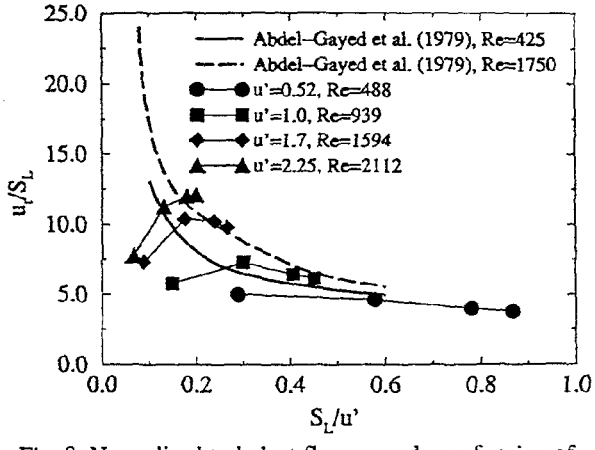

Fig. 8. Normalized turbulent flame speed as a funcion of normalized laminar flame speed for flames B1, B4, B9, and B10, for different *Re* compared with fan-stirred bomb experiments of Abdel-Gayed *et al.*, (1979).